Production of π^+ and K^+ mesons in 3.2 AGeV argon-nucleus interactions at the Nuclotron

BM@N Collaboration

Abstract

First physics results of the BM@N experiment are presented on π^+ and K^+ meson production in interactions of the 3.2 AGeV argon beam with fixed targets. Transverse momentum, rapidity spectra and multiplicities of π^+ and K^+ mesons are measured. The results are compared with predictions of theoretical models and with the measurements from heavy ion experiments at lower energies.

1 Introduction

BM@N (Baryonic Matter at Nuclotron) is the first experiment operational at the Nuclotron/ NICA ion accelerating complex studying relativistic heavy ion beam interactions with fixed targets [1] in the energy range of maximal baryon densities [2]. At the Nuclotron energies the nucleon density in a fireball created by two colliding heavy nuclei is 3-4 times higher than the saturation density [3]. In addition, these energies are high enough to study strange mesons and (multi)-strange hyperons produced in nucleus-nucleus collisions close to the kinematic threshold [4, 5]. The primary goal of the experiment is to constrain parameters of the Equation of State (EoS) of high density nuclear matter. Studies of the excitation function of strange particle production below and close to the kinematical threshold provide the means to differentiate hard from soft behaviour of the EoS [6].

The Nuclotron will provide the experiment with beams of a variety of particles, from protons to gold ions, with a kinetic energy ranging from 1 to 6 GeV/nucleon for light ions with Z/A ratio of 0.5 and up to 4.5 GeV/nucleon for heavy ions with Z/A ratio of 0.4.

Recently BM@N collected first experimental data in beams of carbon, argon, and krypton ions [7, 8]. This paper presents first results on π^+ and K^+ meson production in 3.2 AGeV argon-nucleus interactions based on data that correspond to an integrated luminosity of 7.8 $\mu\mathrm{b}^{-1}$.

The paper is organized as follows. Section 2 describes the experimental set-up and section 3 is devoted to details of the event reconstruction. Section 4 describes the evaluation of the π^+, K^+ reconstruction efficiency. Experimental results on transverse momentum, rapidity spectra and multiplicities of π^+ and K^+ mesons are given in section 5. The BM@N measurements are compared with predictions of theoretical models and with the experimental data on middle-sized nucleus-nucleus interactions measured at lower energies. Finally, the results are summarized in section 6.

2 Experimental set-up

The BM@N detector is a forward spectrometer covering the pseudorapidity range $1.6 \leq \eta \leq 4.4$. A schematic view of the BM@N set-up in the argon beam run is shown in figure 1. Components of the set-up are described in [9]. The spectrometer includes a central tracking system consisting of 3 planes of forward silicon-strip detectors (ST) and 6 planes of detectors based on gas electron multipliers

(GEM) [10]. The central tracking system is located downstream of the target region inside of a dipole magnet with a bending power of about $\approxeq 2.1$Tm.

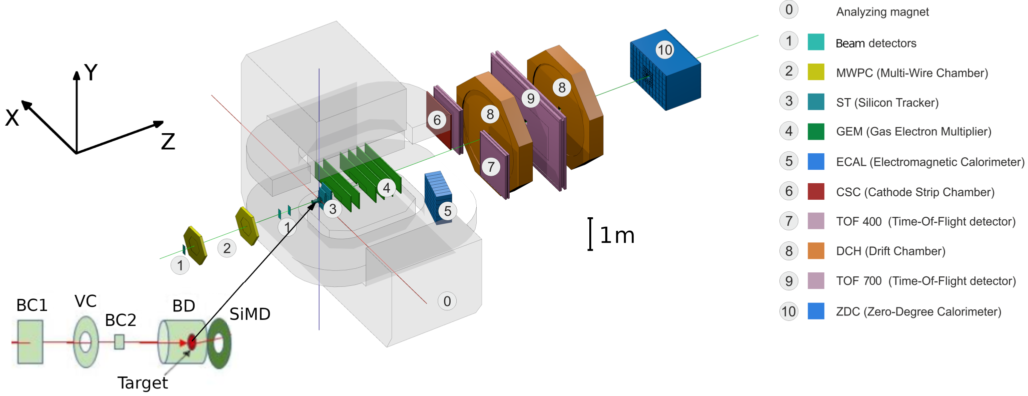

Figure 1: Scheme of the BM@N set-up in the argon beam run.

Outer drift chambers (DCH), a cathode strip chamber (CSC), two sets of time-of-flight detectors (ToF), and a zero degree calorimeter (ZDC) are located downstream the dipole magnet. The tracking system provides a measurement of the momentum, p, of charged particles with a relative uncertainty that varies from 2.5% at the momentum of 0.5 GeV/c to 4.5% at 3.5 GeV/c as it is shown in figure 2.

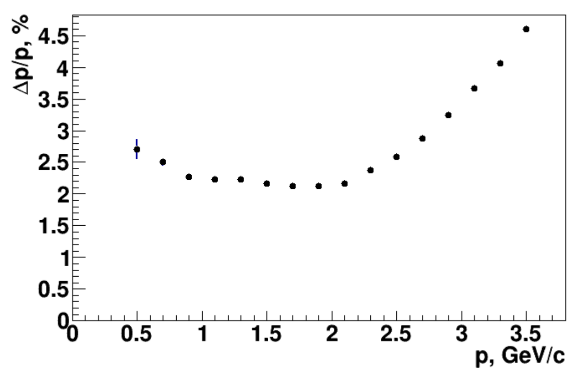

Figure 2: Relative momentum resolution as a function of the momentum.

The minimum distance of a track to a primary nucleus-nucleus collision vertex (PV) is measured with a resolution of 2.4 mm in the X-Y plane. Different types of charged hadrons are identified by two ToF systems.

The online event selection is performed by a trigger, based on two beam counters (BC1, BC2), a veto counter (VC), a barrel detector (BD), and a silicon multiplicity detector (SiMD). The BC2 counter was used as a start trigger T0. The BD detector consists of 40 azimutal strips arranged around the target, and the SiMD detector comprises 60 azimutal segments situated behind the target.

To count the number of beam ions that passed through the target, a logical beam trigger BT = BC1·VC_{veto}· BC2 was used. To form a trigger signal, the following logic was applied: BT·(BD $\geq$ m)·(SiMD $\geq$ n). Different conditions were required on the minimum number of fired channels in the BD detector (m) and the SiMD detector (n), where m and n were ranged from 2 to 4 during the run. The trigger conditions were varied to find the optimal ratio between the event rate and the trigger efficiency for each individual target. The measurements cover the whole range of event centralities, but the trigger efficiency was lower for peripheral interactions than that for central and intermediate collisions.

The data from the forward silicon detectors, GEM detectors, outer drift chambers, cathode strip chamber and two sets of the time-of-flight detectors ToF-400 and ToF-700 were used for the analysis. The acceptances of the ToF-400 [33] and ToF-700 [34] detectors cover different kinematical ranges of the rapidity and transverse momentum of identified particles. The time resolutions of the ToF-400 and ToF-700 systems are 84 ps and 115 ps, respectively [35]. The analyzed statistics of argon-nucleus collisions was 83M events for 3.2 AGeV argon beam data.

The research program of the run was devoted to measurements of inelastic reactions $Ar + A \rightarrow X$ with the argon beam intensity of a few 10^5 ions per spill and a spill duration of 2–2.5 sec. A set of 3% nuclear length solid targets of different materials (C, Al, Cu, Sn, Pb) was used.

3 Event reconstruction

Track reconstruction in the central tracker is based on a “cellular automaton” approach [11] implementing a constrained combinatorial search of track candidates with their subsequent fit by the Kalman filter to produce track parameters. These tracks are used to reconstruct primary (interaction) and secondary (decay) vertices and to build global tracks by extrapolating to downstream detectors (CSC, DCH and ToF) and matching with their measurements.

π^+ and K^+ mesons were identified using the time of flight measured in T0 and ToF detectors, the length of the trajectory and the momentum reconstructed in the central tracker. Candidates to π^+ and K^+ should originate from the primary event vertex, correlate with hits in the CSC (DCH) detectors and match hits in the ToF-400 (ToF-700) detectors. Herewith, the CSC (DCH) hits were used to confirm the quality of the tracks matched to ToF-400 (ToF-700) hits.

The criteria for selection of π^+ and K^+ meson candidates were the following:

- Each track has at least 4 hits in the GEM detectors (6 detectors in total) [10]. Hits in the forward silicon detectors were used for the track reconstruction, but no requirement on the number of hits was applied;

- Tracks are originated from the primary event vertex, the deviation of the reconstructed vertex from the position of the target along the beam direction is limited to -3.4 cm $< Z_{ver} - Z_0 <$ 1.7 cm, where Z_0 is the target position. The upper limit corresponds to 7σ of the Z_{ver} spread and cuts off interactions with the trigger detector situated at 3 cm behind the target (see figure 7e);

- Distance from a track to the primary event vertex in the X-Y plane at Z$_{ver}$ (DCA) is required to be less than 1 cm, which corresponds to 4 σ of the vertex resolution in the X-Y plane;

- Momentum range of positive tracks $p > 0.5, 0.7$ GeV/c is limited by the acceptance of the ToF-400 and ToF-700 detectors, respectively;

- Distance of extrapolated tracks to the CSC (DCH) hits as well as to the ToF-400 (ToF-700) hits should be within $\pm 2.5\sigma$ of the hit-track residual distributions and depends upon the track momentum range as shown in figure 3.

The distribution of the primary vertices along the beam direction (Z_{ver}) for experimental data and Monte Carlo events is shown in figure 7e. Two vertical lines limit the region of the Z coordinate accepted for the data analysis for all the targets.

Spectra of the mass squared (M^2) of positive particles produced in interactions of the 3.2 AGeV argon beam with different targets are shown in figure 4a and 4b for ToF-400 and ToF-700 data, respectively. Signals of π^+ and K^+ were extracted in windows of M^2 from -0.09 to 0.13 (GeV/c^2)^2 and from 0.18 to 0.32 (GeV/c^2)^2, respectively. The π^+ and K^+ signals and statistical errors were calculated according to the formulae: $sig = hist - bg$, $err_{stat} = \sqrt{hist + bg}$, assuming the background uncertainty of $\sqrt{bg}$. Here $hist$ and bg denote the histogram integral and the background integral within the M^2 windows of π^+ and K^+ mesons.

(a) (b)

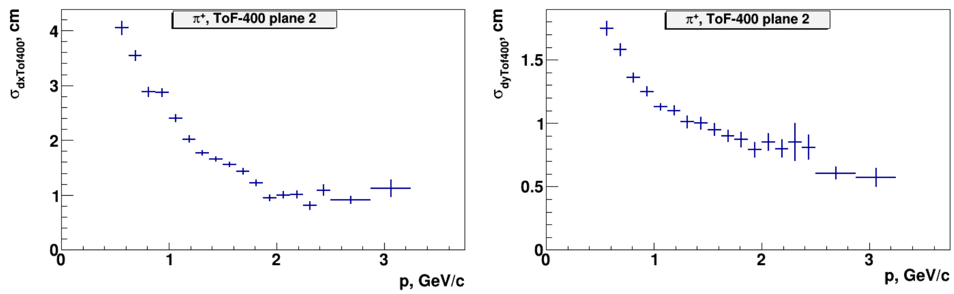

Figure 3: Sigma of residuals of the ToF-400 hits with respect to positive tracks in dependence on the particle momentum: projection X (a), Y (b).

(a) (b)

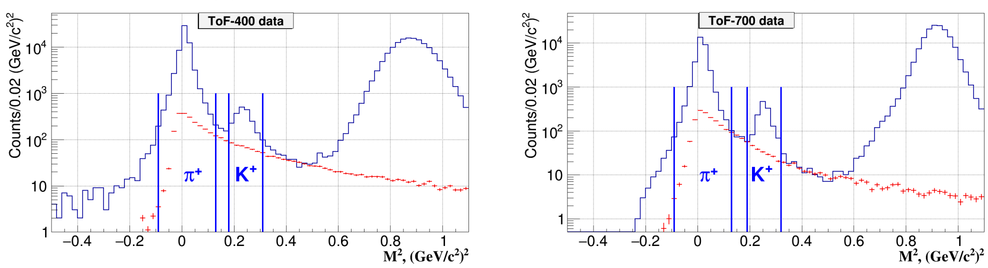

Figure 4: M^2 spectra of positive particles produced in argon-nucleus interactions and measured in the ToF-400 (a) and ToF-700 (b) detectors. Vertical lines show the signal ranges of identified π^+ and K^+ mesons. Red points with the error bars show the the background estimated from "mixed" events.

To estimate the background under the π^+ and K^+ signals, a "mixed event" method was used, i.e. the shape of the M^2 background distribution was evaluated by matching tracks to hits in the ToF-400 and ToF-700 detectors originated from independent events. To estimate the π^+ and K^+ signal systematic errors due to the background subtraction method, the M^2 distributions were parameterized using a linear fit in the M^2 range -0.14-0.4 (GeV/c^2)^2. The M^2 windows of the π^+ and K^+ signals were excluded from the linear fit. The variation of the background integral under the π^+ and K^+ signals taken from mixed events relative to the bg integral taken from the fit of the M^2 spectra was treated as a systematic error.

The fraction of fake combinations of tracks and hits in the ToF detectors was evaluated by the "mixed event" method described above. The "mixed event" fraction was found to differ for interactions of the beam with light and heavy targets and for different bins of the transverse momentum and rapidity.

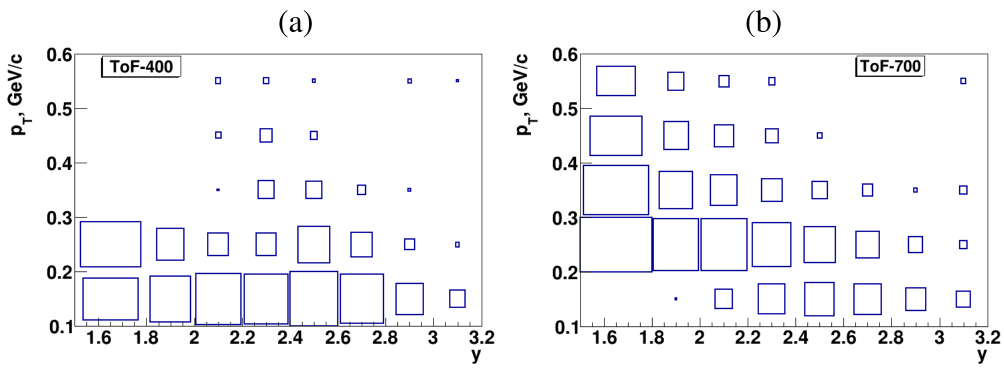

Figure 5: Distribution of the π^+ signals measured in ToF-400 (a) and ToF-700 (b) in the rapidity and transverse momentum bins in Ar+Sn interactions.

Figure 5 shows the phase-space coverage of the π^+ signals measured in ToF-400 and ToF-700 in the intervals of rapidity and transverse momentum in Ar+Sn interactions before the efficiency corrections.

4 Reconstruction efficiency

Monte Carlo data samples of argon-nucleus collisions were produced with the DCM-SMM event generator [12, 13]. Propagation of particles through the set-up volume and response of the detectors were simulated using the GEANT3 program [14] integrated into the BmnRoot software framework [15]. To properly describe the GEM detector response in the magnetic field, the micro-simulation package Garfield++ [16] was used.

The efficiencies of the forward silicon, GEM, CSC, DCH and ToF detectors were adjusted in simulation to the detector efficiencies measured in experimental events. The Monte Carlo events passed through the same reconstruction and identification chain as experimental events.

The level of agreement between the Monte Carlo and experimental distributions is demonstrated on a set of observables: hit-track residuals in the central tracker detectors, DCA, χ^2/NDF, number of tracks reconstructed in the primary vertex, and number of hits per track (see figure 6 and 7a–d).

The π^+ and K^+ reconstruction efficiency is evaluated in intervals of the rapidity y and transverse momentum p_T. It takes into account the geometrical acceptance, the detector efficiency, the efficiency of kinematic, spatial cuts and the losses of π^+ and K^+ due to decays on flight. The reconstruction efficiencies of π^+

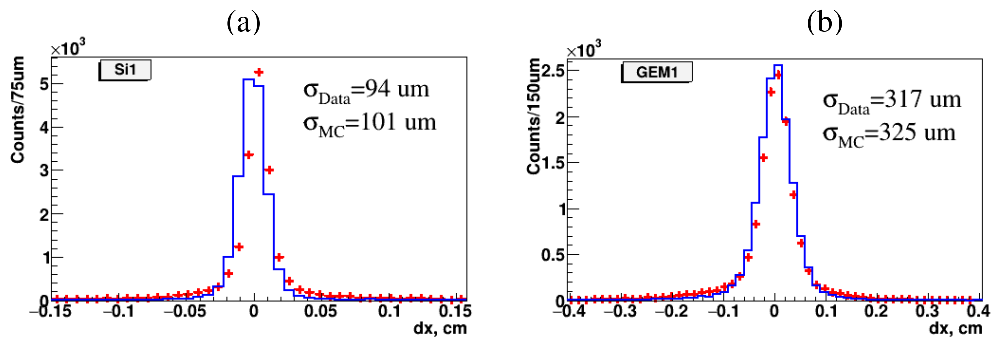

Figure 6: Residual distributions of hits in the X projection (magnet deflection plane) with respect to reconstructed tracks: (a) - in the first forward silicon plane, (b) - in the first GEM plane. Experimental data are shown as red crosses, and simulated data are shown as blue histograms.

detected in ToF-400 and ToF-700 are shown in figure 8 in the y and p_T intervals for Ar+Sn interactions.

The efficiency to get a trigger signal based on multiplicities of fired channels in the BD (SiMD) detectors ϵ_{trig} was calculated for events with reconstructed π^+ and K^+ mesons using experimental event samples recorded with an independent trigger based on the SiMD (BD) detectors: ϵ_{trig} (BD $\geq$ m) = N(BD $\geq$ m, SiMD $\geq$ n)/ N(SiMD $\geq$ n) , where m and n are the minimum number of fired channels in BD and SiMD varied in the range from 2 to 4. The dependences of the trigger efficiency on the track multiplicity in the primary event vertex and the X/Y vertex position were taken into account. The efficiency for the combined BD and SiMD triggers was calculated as a product of the BD and SiMD trigger efficiencies. The systematic errors evaluated in the analysis cover the differences in the π^+, K^+ signals obtained by using the mean values of the trigger efficiency values instead of the efficiency dependences on the number of vertex tracks and primary vertex position.

5 Results

The differential cross sections $d^2\sigma_{\pi,K}(y,p_T)/dydp_T$ and yields $d^2N_{\pi,K}(y,p_T)/dydp_T$ of π^+ and K^+ meson production in Ar+C, Al, Cu, Sn, Pb interactions are calculated in bins of (y,p_T) according to the formulae:

$$d^2\sigma_{\pi,K}(y,p_T)/dydp_T = n_{\pi,K}(y,p_T)/dydp_T/(\epsilon_{rec}(y,p_T)\cdot\epsilon_{trig}\cdot L)$$

$$d^2N_{\pi,K}(y,p_T)/dydp_T = d^2\sigma_{\pi,K}(y,p_T)/dydp_T/\sigma_{inel} \quad (1)$$

where L is the luminosity, $n_{\pi,K}$ is the number of reconstructed π^+ and K^+ mesons in intervals dy and dp_T, ϵ_{rec} is the efficiency of the π^+ and K^+ meson reconstruction, ϵ_{trig} is the trigger efficiency, σ_{inel} is the cross section for minimum bias inelastic argon-nucleus interactions. The cross sections for inelastic Ar+C, Al, Cu, Sn, Pb interactions are taken from the predictions of the DCM-SMM model which are consistent with the results calculated by the formula: $\sigma_{inel} = \pi R_0^2(A_P^{1/3} + A_T^{1/3})^2$, where $R_0 = 1.2$ fm is the effective nucleon radius, A_P and A_T are the atomic numbers of the projectile and target nucleus [29]. The uncertainties for the Ar+C, Al, Cu, Sn, Pb inelastic cross sections are estimated from the alternative formula ([20]): $\sigma_{inel} = \pi R_0^2(A_P^{1/3} + A_T^{1/3} - b)^2$ with $R_0 = 1.46$ fm and $b = 1.21$ The values and uncertainties of σ_{inel} for Ar+C, Al, Cu, Sn, Pb interactions used to evaluate the π^+ and K^+ meson yields are given in table 2.

The yields of π^+ (K^+) mesons in Ar+C, Al, Cu, Sn, Pb interactions are measured in the kinematic range of the π^+ (K^+) meson transverse momentum $0.1 < p_T < 0.6$ GeV/c ($0.1 < p_T < 0.5$ GeV/c) and the π^+ (K^+) meson rapidity in the laboratory frame $1.5 < y < 3.2$ ($1.0 < y < 2.0$). The systematic error of the π^+ and K^+ meson yield in every p_T and y bin is calculated as a quadratic sum of uncertainties coming from the following sources:

- Sys1: systematic errors of the reconstruction efficiency due to the remaining difference in the X/Y primary vertex distribution in the simulation relative to the experimental data.

- Sys2: systematic errors of the background subtraction under the π^+ and K^+ signals in the mass squared spectra of identified particles as described in section 3.

- Sys3: systematic error of the trigger efficiency evaluated as a function of the number of tracks from the primary vertex and the X/Y primary vertex position.

The π^+ and K^+ meson yield normalization uncertainties are calculated for the whole measured (y, p_T) range as a quadratic sum of the statistical uncertainty of the trigger efficiency, uncertainties of the tracking detector efficiency, efficiency of the track matching to the CSC (DCH) outer detectors and to ToF-400 (ToF-700), uncertainties of the luminosity and inelastic nucleus-nucleus cross section. The luminosity uncertainty is estimated to be within 2%. The statistical uncertainty of the trigger efficiency is 28% for K^+ detection in Ar+C interactions and between

7.5% (Ar+Al) and 4% (Ar+Pb) for K^+ detection in interactions of argon ions with heavier targets. The trigger efficiency uncertainty for π^+ detection ranges between 4.5% (Ar+C) and 0.9% (Ar+Pb). The uncertainty of the central tracking detector efficiency is estimated to be within 3%. The combined uncertainty of matching of extrapolated tracks to the CSC (DCH) hits and ToF-400 (ToF-700) hits is within 5%. Table 1 summarizes the total systematic uncertainty originated from sources Sis1 - Sis3 and the normalization uncertainty of the π^+ and K^+ yields.

Table 1: Systematic uncertainties of the π^+ and K^+ yields measured in argon-nucleus interactions.

Reaction / Systematics	Ar+C sys%	Ar+Al sys%	Ar+Cu sys%	Ar+Sn sys%	Ar+Pb sys%
Sys1-Sys3, π^+	14	11	12	9	9
Norm (trigger + tracking + luminosity), π^+	7.8	6.3	6.2	6.2	6.2
Sys1-Sys3, K^+	28	26	14	12	16
Norm (trigger + tracking + luminosity), K^+	29	10	8.4	7.6	7.4

The differential y spectra of the π^+ and K^+ meson yields are calculated in the p_T bins using formulae (1) and presented in figure 9 and 10, respectively. The measurements correspond to the forward and central rapidity range in the nucleon-nucleon CM system because the rapidity of the beam-target nucleon-nucleon CM system is $y_{CM} = 1.08$ for the 3.2 GeV/nucleon beam kinetic energy. The predictions of the DCM-SMM [12, 13], UrQMD [18] and PHSD [19] models are shown for comparison. Although the DCM-SMM model was used to evaluate the reconstruction efficiency (section 4), the model predictions could differ from the measurement results. All three models predict more flat behaviour of the π^+ spectra as a function of rapidity at low p_T in comparison with the experiment. The experimental π^+ spectra are a factor of 1.5 lower of the model predictions for π^+ production in Ar+C interactions. All three models predict higher multiplicities of K^+ at low p_T than measured in the experiment. But the difference is smaller at larger values of p_T. The DCM-SMM model predicts higher multiplicities of K^+ at low p_T and rapidity compared to PHSD, whereas the UrQMD predictions are below PHSD at low p_T. The invariant differential p_T spectra of the π^+ and K^+ meson yields are measured in the bins of rapidity y and presented in figure 11 and 12, respectively. Due to low statistics of the K^+ meson signal in Ar+C interactions, the results are given only for the whole measured range in y and p_T. The invariant differential p_T spectra of the K^+ meson yields in the whole measured rapidity range are presented in figure 13. In figure 11, 12 and 13 the measured invariant differential p_T spectra of the π^+ and K^+ meson yields are parameterized by the form: $1/p_T \cdot d^2N/dydp_T \propto \exp(-(m_T - m_{\pi,K})/T_0)$, where $m_T = \sqrt{m_{\pi,K}^2 + p_T^2}$ is the transverse mass, dy is the width of the measured y bin, dp_T is the width of the measured p_T bin, the inverse slope parameter T_0 is a free parameter of the fit. The values of the inverse slope T_0, extracted from the fits of the invariant p_T spectra of π^+ and K^+ mesons are given in figure 14 and 15, respectively. The value of T_0 measured for π^+ mesons produced in argon-nucleus interactions at the beam kinetic energy of 3.2 AGeV is about 40 MeV in the forward rapidity range, rising up to 90 MeV in the central rapidity range. In general, the y dependence of the fit results for π^+ mesons is consistent with the predictions of the DCM-SMM, UrQMD and PHSD models, but there is a tendency that BM@N measures a flatter dependence of the T_0 values in the central rapidity range compared to a rising dependence of the inverse slopes predicted by the models. The T_0 slope values measured in 3 y bins for K^+ mesons have large statistical and systematic errors (see figure 15), but the slope dependence on y is rather weak. The T_0 values obtained for the whole measured range of $1.0 < y < 2.0$ are consistent within the errors with 80 MeV for all the targets (see table 3). Weak y dependence of the T_0 slope is reproduced by all three models, but UrQMD predicts a factor of 2 larger values of the slope compared to the measurement. The measured values of yields (multiplicities) of π^+ and K^+ mesons in Ar+C, Al, Cu, Sn, Pb interactions are extrapolated to the full kinematic range using the averaged values of the extrapolation factors from predictions of the DCM-SMM, UrQMD and PHSD models which are given in table 2. The RMS of differences between the model predictions are taken as the model uncertainties of the extrapolation factors. The π^+ and K^+ meson multiplicities and the ratios of the K^+ to π^+ meson multiplicities are summarized in table 3. The ratios of the K^+ to π^+ multiplicities show no significant dependence on the mean number of nucleons-participants of argon-nucleus collisions A_{part} given in table 2. The A_{part} values are calculated from predictions of the DCM-SMM model.

The BM@N results on the π^+ and K^+ multiplicities are compared with predictions of the DCM-SMM, UrQMD and PHSD models in figure 16a,b. The measured ratios of the π^+ and K^+ meson multiplicities to $A_{\rm part}$ decrease with the target atomic weight from Al to Pb. The result for π^+ in Ar+C interactions is below the results for heavier targets. The ratios of the K^+ to π^+ multiplicities are given in figure 16c. They show no dependence on the number of nucleons-participants, whereas the models predict smooth rising of the K^+ to π^+ ratio with $A_{\rm part}$.

The π^+ and K^+ meson multiplicities in argon-nucleus interactions can be compared with the previous results of the HADES experiment measured Ar+KCl interactions at the lower beam kinetic energy of 1.76 AGeV [21–23] and with the FOPI experiment measured Ni+Ni interactions at the beam kinetic energy of 1.93 AGeV [24–26]. The KaoS experiment also measured the K^+ multiplicities in Ni+Ni interactions at the beam kinetic energies of 1.5 and 1.93 AGeV [27, 28] which are consistent with the results of the FOPI experiment. The HADES experiment measured the total multiplicities of π^- and K^+ in semi-central events (the mean number of nucleons-participants $A_{\rm part}$ of 38.5) of 3.9 and $2.8 \cdot 10^{-2}$, respectively. The effective inverse slope parameters of the m_T spectra of π^- and K^+ extrapolated to $y^* = 0$ are 82.4 MeV and 89 MeV, respectively. The BM@N results on the K^+ and π^+ multiplicities at the beam kinetic energy of 3.2 AGeV in Ar+Cu interactions ($A_{\rm part}$ of 33.6, see table 2) are higher by factors of 3.5 and 1.3 relative to the results for kaons and pions measured by HADES. The inverse slope parameters T_0 measured for π^+ and K^+ in the central rapidity range (see figure 14 and 15) are comparable with the results of HADES.

The FOPI experiment measured the total multiplicities of K^+ in triggered semi-central Ni+Ni interactions ($A_{\rm part}$ of 46.5) and central events ($A_{\rm part}$ of 75) of $3.6 \cdot 10^{-2}$ and $8.25 \cdot 10^{-2}$, respectively. These values could be compared with the BM@N results presented in table 3 for different targets. The K^+/π^+ multiplicity ratio measured by FOPI in triggered semi-central events is $7.6 \cdot 10^{-3}$, which is a factor 3 smaller than the K^+/π^+ multiplicity ratio obtained by BM@N in Ar + Sn interactions for the full kinematical range ($A_{\rm part}$ of 48.3, see table 2). It should be taken into account that the beam kinetic energy of the FOPI experiment (1.93 AGeV) is lower than that of the BM@N experiment. The effective inverse slope of 110.9 MeV evaluated by FOPI at $y^* = 0$ from the K^+ transverse mass spectrum is consistent within the uncertainties with the inverse slope parameter T_0 measured by BM@N for K^+ in the range $y^* \gtrsim 0$.

The pion multiplicities in the full kinematic range N_{π}^{tot}, where $N_{\pi}^{tot} = N_{\pi^+}^{tot} + N_{\pi^-}^{tot} + N_{\pi^0}^{tot}$ normalized to the mean number of nucleons-participants $A_{\rm part}$ are compiled in figure 17 for different colliding nucleus and beam energies. The reference [36] contains the pion data for N+N [38], Mg+Mg [39], La+La [40], Au+Au [41–43], Ar+KCl [44], Si+Al, S+S [45, 46], Pb+Pb [47]. The reference [37] compiles the pion data for Au+Au [48–51]. To estimate N_{π}^{tot} from the π^{+} multiplicities measured by BM@N, the predictions of the DCM-SMM model w ere used. The K^{+} multiplicities in the full kinematic range normalized to the mean number of nucleons-participants $A_{\rm part}$ are compiled in figure 18. The world data taken from [24, 52–55] are compared with the results of the BM@N experiment. Figures 17 and 18 show that the BM@N results are consistent with the world data on π and K^{+} production.

6 Summary

First physics results of the BM@N experiment are presented on the π^{+} and K^{+} meson yields and their ratios in argon-nucleus interactions at the beam kinetic energy of 3.2 AGeV. The results are compared with the models of nucleus-nucleus interactions and with the results of other experiments studied nucleus-nucleus interactions at different energies.

Acknowledgments. The BM@N Collaboration acknowledges support of the HybriLIT of JINR, HPC Village project and HGPU group for the computational resources provided. This work is supported by the Russian Foundation for Basic Research (RFBR) under grant No. 18-02-40036 mega.

References

[1] M. Kapishin (for the BM@N Collaboration), Eur. Phys. J. A52 (2016) no. 8, 213.

[2] J. Randrup and J. Cleymans, Phys. Rev. C 74 (2006) 047901.

[3] B. Friman, W. Nörenberg, and V.D. Toneev, Eur. Phys. J. A 3 (1998).

[4] NICA White Paper, Eur. Phys. J. A 52 (2016).

[5] BM@N Conceptual Design Report:
http://nica.jinr.ru/files/BM@N/BMN_CDR.pdf

[6] Ch. Fuchs, Prog. Part. Nucl. Phys. 56 (2006) 1-103.

[7] M. Kapishin (for the BM@N Collaboration), Nucl. Phys. A 982 (2019) 967-970.

[8] M. Kapishin (for the BM@N Collaboration), SQM 2019 proceedings, 285 Springer Proc. Phys. 250 (2020) 21-27.

[9] BM@N project:
http://nica.jinr.ru/files/BM@N/BMN_project.pdf

[10] D. Baranov et al., JINST 12 (2017) no. 06, C06041 .

[11] V. Akishina and I. Kisel, J. Phys.: Conf. Ser. 599, 012024 (2015), I. Kisel, Nucl. Instrum. Meth. A 566, 85 (2006).

[12] N. Amelin, K. Gudima, and V. Toneev, Sov. J. Nucl. Phys. 51, 1093 (1990).

[13] M. Baznat, A. Botvina, G. Musulmanbekov, V. Toneev, V. Zhezher, Phys. Part. Nucl. Lett. 17 (2020) no. 3; arXiv: 1912.09277v.

[14] CERN Program Library, Long Writeup W5013, Geneva, CERN, 1993.

[15] https://git.jinr.ru/nica/bmnroot

[16] http://garfieldpp.web.cern.ch/garfieldpp

[17] D. Baranov et al., Phys. Part. Nucl. Lett. 15 (2018) no. 2, 148-156.

[18] S. A. Bass et al., Prog. Part. Nucl. Phys. 41 225 (1998).

[19] W. Cassing and E. L. Bratkovskaya, Nucl. Phys. A 831 (2009) 215-242.

[20] H. Angelov et al., P1-80-473, JINR, Dubna.

[21] G. Agakishiev et al., HADES Collaboration, Eur. Phys. J. A 47 (2011) 21.

[22] G. Agakishiev et al., HADES Collaboration, Phys. Rev. C 80 (2009) 025209.

[23] G. Agakishiev et al., HADES Collaboration, Phys. Rev. C 82 (2010) 044907.

[24] D. Best et al., FOPI Collaboration, Nucl. Phys. A 625 (1997) 307-324.

[25] N. Bastid et al., FOPI Collaboration, Phys. Rev. C 76 (2007) 024906.

[26] K. Piasecki et al., FOPI Collaboration, Phys. Rev. C 99 (2019) 1, 014904.

[27] M. Menzel et al., KaoS Collaboration, Phys. Lett. B 495 (2000) 26-32.

[28] A. Forster et al., KaoS Collaboration, Phys. Rev. C 75 (2007) 024906.

[29] K. Kanaki, PhD Thesis, Technische Universität Dresden, 2007.

[30] Yu. Kovalev et al., 2017 JINST 12 C07031; B. Topko et al., in IEEE Transactions on Nuclear Science, vol. 69, no. 1, pp. 98-104, Jan. 2022; Topko, B. L. et al., Phys. Part. Nuclei 53, 639–643 (2022); Yu. Topko et al., Nucl. Instrum. Meth. A 1033, 166680 (2022) .

[31] A. Galavanov et al., EPJ Web Conf. 204 (2019) 07009; A. Galavanov et al., 2020 JINST15 C09038.

[32] M. Kapishin et al., EPJ Web Conf., 173 (2018) 04008; E. Mazzucato, Nucl. Phys. B 59 (1997) 174-181.

[33] V. Babkin et al., Nucl. Instrum. Meth. A 824, P.490–492 (2016); V. Babkin et al., Proceedings of Science, 2014, Vol.213 (Proceedings of TIPP-2014), P.289 .

[34] N. Kuzmin et al., Nucl. Instrum. Meth. A 916, P. 190–194 (2019) .

[35] K. Alishina et al., Phys. Part. Nucl., 53 (2022) no. 2, 470-475.

[36] P. Senger et al., J. Phys. G 25 (1999) R59-R131.

[37] J. Adamczewski-Musch et al., Eur. Phys. J. A 56 (2020) 259.

[38] Gazdzicki M. and Röhrich D., 1995 Z. Phys. C 65 215.

[39] Anikina et al., JINR Rapid Comm Dubna, 1 (1989) 12.

[40] Harris J. W. et al., 1987 Phys. Rev. Lett. 58 463.

[41] Pelte D. et al., 1997 Z. Phys. A 357 215.

[42] Wagner A. et al., 1998 Phys. Lett. B 420 20.

[43] Schwalb O. et al., 1994 Phys. Lett. B 321 20.

[44] Harris J. W. et al., 1985 Phys. Lett. B 153 377.

[45] T. Abbott et al. (E-802 Collaboration), Phys. Rev. C 50 (1993) 1024.

[46] J. Bachler et al., Phys. Rev. Lett. 72 (1994) 1419.

[47] Jacobs P. and NA49 Collaboration 1997 Proc. of the 3rd Int. Conf. on the Physics and Astrophysics of the Quark Gluon Plasma (Jaipur, India) (Delhi: Narosa).

[48] W. Reisdorf et al. (FOPI Collaboration), Nucl. Phys. A 781, 459 (2007).

[49] A.R. Wolf et al. (TAPS Collaboration), Phys. Rev. Lett. 80, 5281 (1998).

[50] R. Averbeck et al., Phys. Rev. C 67, 024903 (2003).

[51] J.L. Klay et al. (E895 Collaboration), Phys. Rev. C 68, 054905 (2003).

[52] R. Barth et al. Phys. Rev. Lett. 78 (1997), p. 4007.

[53] L. Ahle et al. (E802 Collaboration), Phys. Rev. C 60, 044904 (1999).

[54] L. Ahle et al. (E802 Collaboration), Phys. Rev. C 58, 3523 (1998).

[55] Afanasiev S. V. et al., Phys. Rev. C. 66 054902 (2002).

Table 2: 1) Extrapolation factors for π^+ and K^+ meson multiplicities from the measured range to the full kinematical range. The factors are averaged over predictions of the DCM-SMM, PHSD, UrQMD models. The errors are RMS of differences in the model predictions. 2) Number of nucleons-participants from predictions of the DCM-SMM model. 3) Inclusive cross sections for inelastic Ar+A interactions.

3.2 AGeV argon beam	Ar+C	Ar+Al	Ar+Cu	Ar+Sn	Ar+Pb
Extrap. factor for π^+	3.25 ± 0.14	3.73 ± 0.1	4.45 ± 0.06	5.12 ± 0.18	5.91 ± 0.4
Extrap. factor for K^+	2.81 ± 0.49	3.02 ± 0.48	3.34 ± 0.48	3.7 ± 0.43	4.1 ± 0.35
A_{part}, DCM-SMM	14.8	23.0	33.6	48.3	63.6
σ_{inel}, mb [29]	1470 ± 50	1860 ± 50	2480 ± 50	3140 ± 50	3940 ± 50

Table 3: π^+ and K^+ meson multiplicities measured in Ar+C, Al, Cu, Sn, Pb interactions at the argon beam energy of 3.2 AGeV. The first error given is statistical, the second error is systematic. The third error given for the full π^+ and K^+ multiplicities is the model uncertainty.

3.2 AGeV argon beam	Ar+C	Ar+Al	Ar+Cu	Ar+Sn	Ar+Pb
Measured π^+ mult. $N_{\pi+}$	$0.42 \pm 0.008 \pm 0.045$	$1.00 \pm 0.01 \pm 0.07$	$1.14 \pm 0.01 \pm 0.08$	$1.28 \pm 0.01 \pm 0.09$	$1.25 \pm 0.01 \pm 0.08$
Measured K^+ mult. $N_{K+}/10^{-2}$	$1.59 \pm 0.29 \pm 0.65$	$3.90 \pm 0.28 \pm 0.61$	$4.17 \pm 0.21 \pm 0.66$	$5.60 \pm 0.22 \pm 0.75$	$5.10 \pm 0.22 \pm 0.92$
Full π^+ mult. $N_{\pi+}^{tot}$	$1.365 \pm 0.026 \pm 0.146 \pm 0.06$	$3.73 \pm 0.04 \pm 0.26 \pm 0.1$	$5.07 \pm 0.04 \pm 0.36 \pm 0.07$	$6.55 \pm 0.05 \pm 0.46 \pm 0.23$	$7.39 \pm 0.06 \pm 0.47 \pm 0.5$
Full K^+ mult. $N_{K+}^{tot}/10^{-2}$	$4.47 \pm 0.81 \pm 1.83 \pm 0.77$	$11.8 \pm 0.9 \pm 1.8 \pm 1.9$	$13.9 \pm 0.7 \pm 2.2 \pm 2$	$20.7 \pm 0.8 \pm 2.8 \pm 2.4$	$20.9 \pm 0.9 \pm 3.8 \pm 1.8$
$N_{K+}/N_{\pi+}/10^{-2}$ Measured range	$3.79 \pm 0.69 \pm 1.52$	$3.90 \pm 0.28 \pm 0.55$	$3.66 \pm 0.19 \pm 0.53$	$4.39 \pm 0.18 \pm 0.51$	$4.11 \pm 0.18 \pm 0.68$
$N_{K+}^{tot}/N_{\pi+}^{tot}$ $/10^{-2}$, Full kin. range	$3.27 \pm 0.6 \pm 1.38 \pm 0.58$	$3.16 \pm 0.23 \pm 0.54 \pm 0.51$	$2.75 \pm 0.14 \pm 0.48 \pm 0.39$	$3.16 \pm 0.13 \pm 0.48 \pm 0.39$	$2.83 \pm 0.12 \pm 0.54 \pm 0.31$
K^+ inv. slope T_0, MeV, Meas. range	$67 \pm 12 \pm 12$	$80 \pm 7 \pm 5$	$81 \pm 5 \pm 5$	$81 \pm 5 \pm 4$	$78 \pm 5 \pm 4$

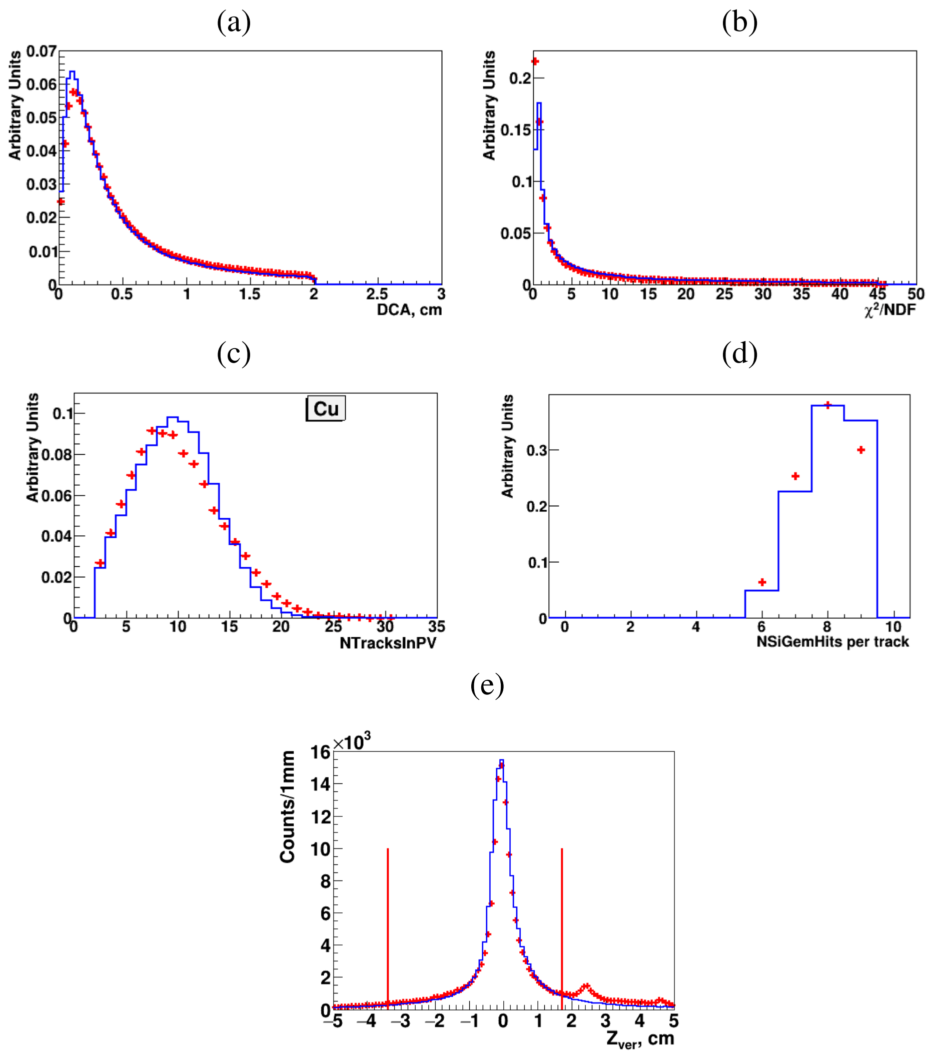

Figure 7: Ar+A interactions at 3.2 AGeV : comparison of the experimental distributions (red crosses) and reconstructed Monte Carlo GEANT distributions of events generated with the DCM-SMM model (blue lines): DCA; χ^2/NDF of reconstructed tracks; number of tracks reconstructed in the primary vertex; number of hits per track reconstructed in 3 forward silicon and 6 GEM detectors; primary vertices along the Z axis for data and simulated events (vertical lines limit the Z region accepted for the data analysis).

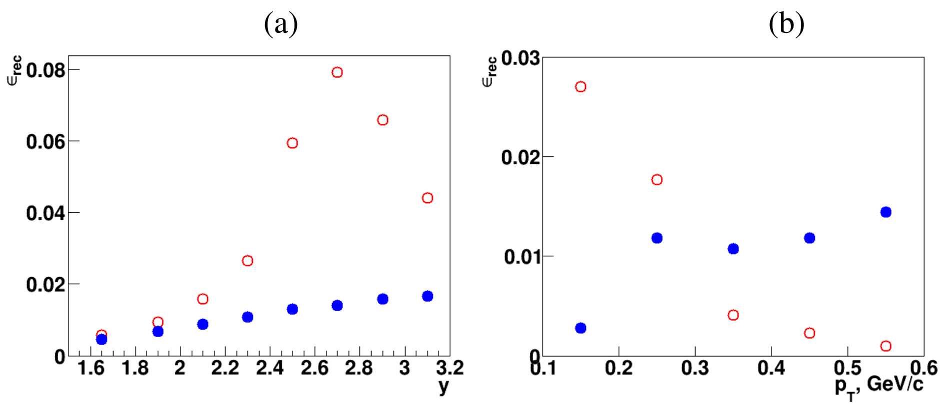

Figure 8: Reconstruction efficiency of π^+ detected in ToF-400 (open red circles) and ToF-700 (full blue circles), calculated as a product of the geometrical acceptance, detector efficiency and efficiency of kinematic and spatial cuts in bins of the rapidity y in the laboratory frame (a) and in bins of p_T (b). The results are shown for π^+ mesons produced in Ar+Sn interactions.

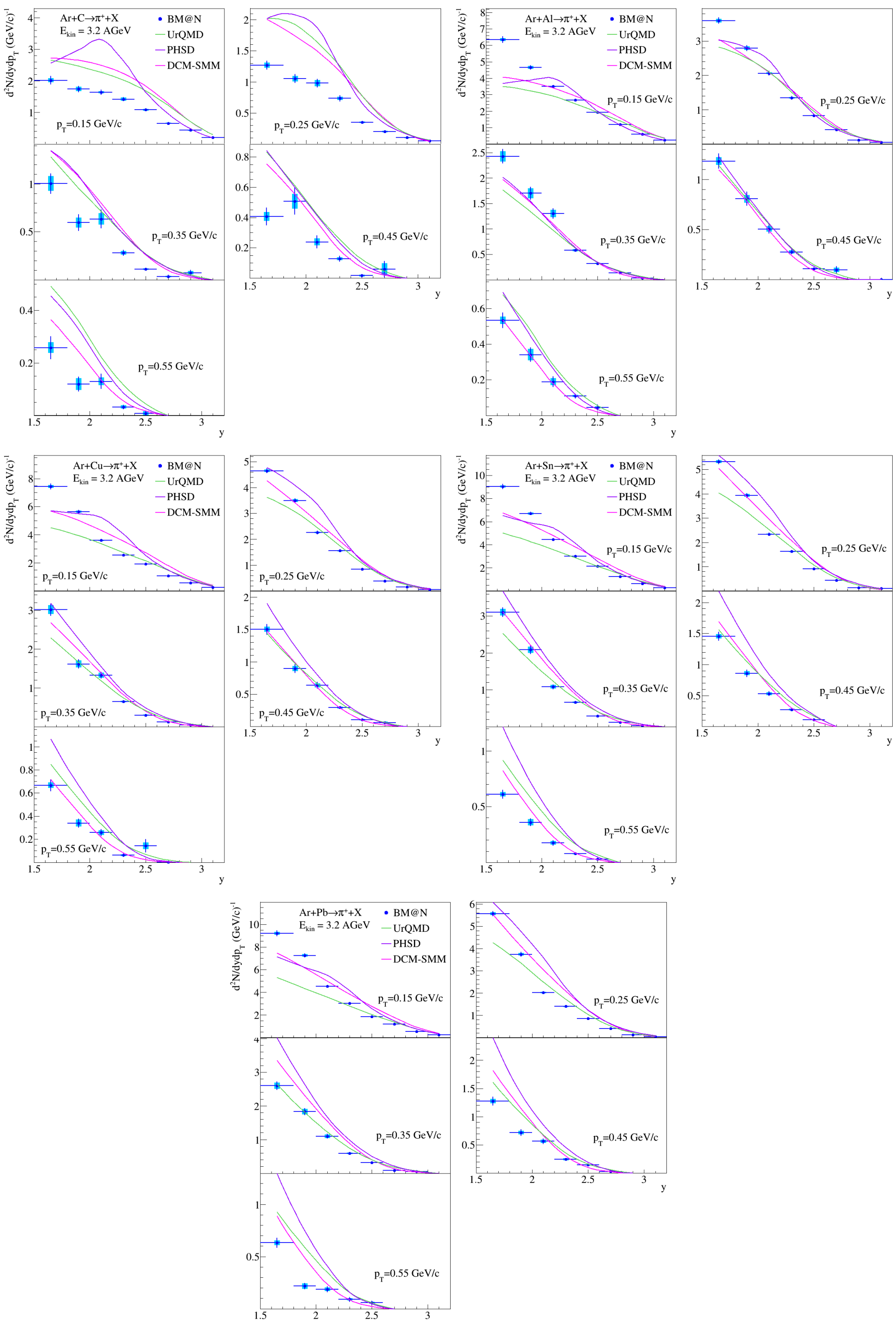

Figure 9: Rapidity spectra (y) of π^+ mesons produced in Ar+C, Al, Cu, Sn, Pb interactions at the argon beam energy of 3.2 AGeV. The results are given for bins of π^+ meson transverse momentum. The error bars represent the statistical errors, the boxes show the systematic errors. The predictions of the DCM-SMM, UrQMD and PHSD models are shown as rose, green and magenta lines.

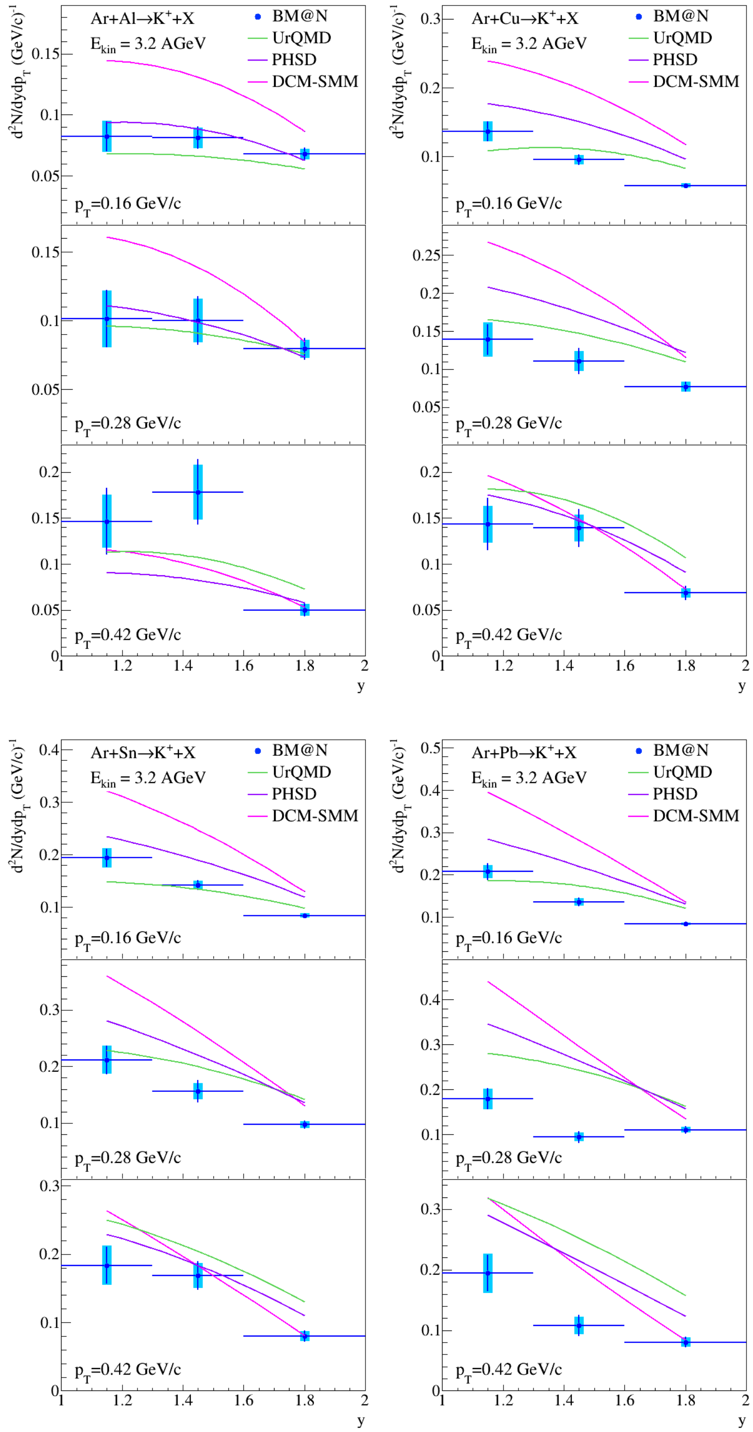

Figure 10: Rapidity spectra (y) of K^+ mesons produced in Ar+Al, Cu, Sn, Pb interactions at the argon beam energy of 3.2 AGeV. The results are given for bins of K^+ meson transverse momentum. The error bars represent the statistical errors, the boxes show the systematic errors. The predictions of the DCM-SMM, UrQMD and PHSD models are shown as rose, green and magenta lines.

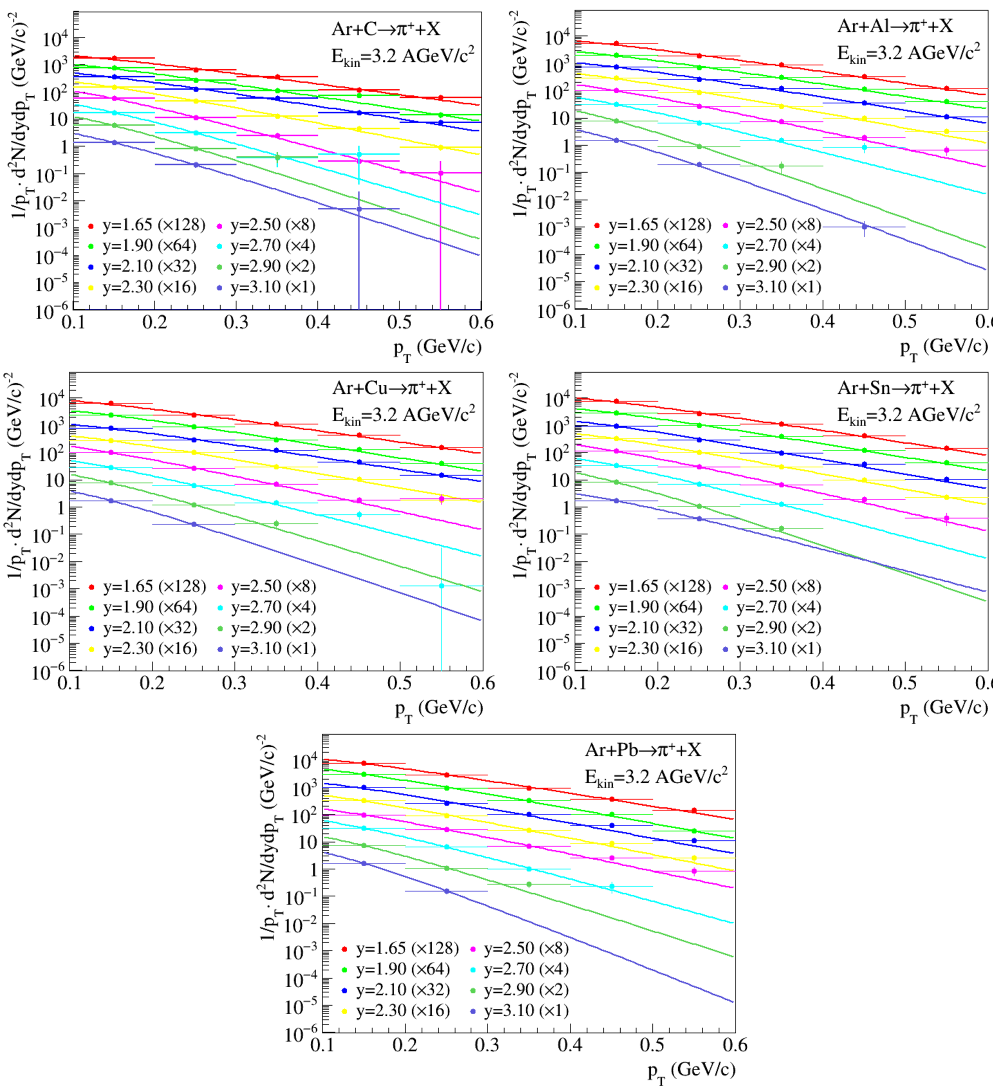

Figure 11: Invariant transverse momentum spectra (p_T) of π^+ mesons produced in Ar+C, Al, Cu, Sn, Pb interactions at the argon beam energy of 3.2 AGeV. The results are given for bins of π^+ meson rapidity. The lines represent the results of the parameterization described in the text.

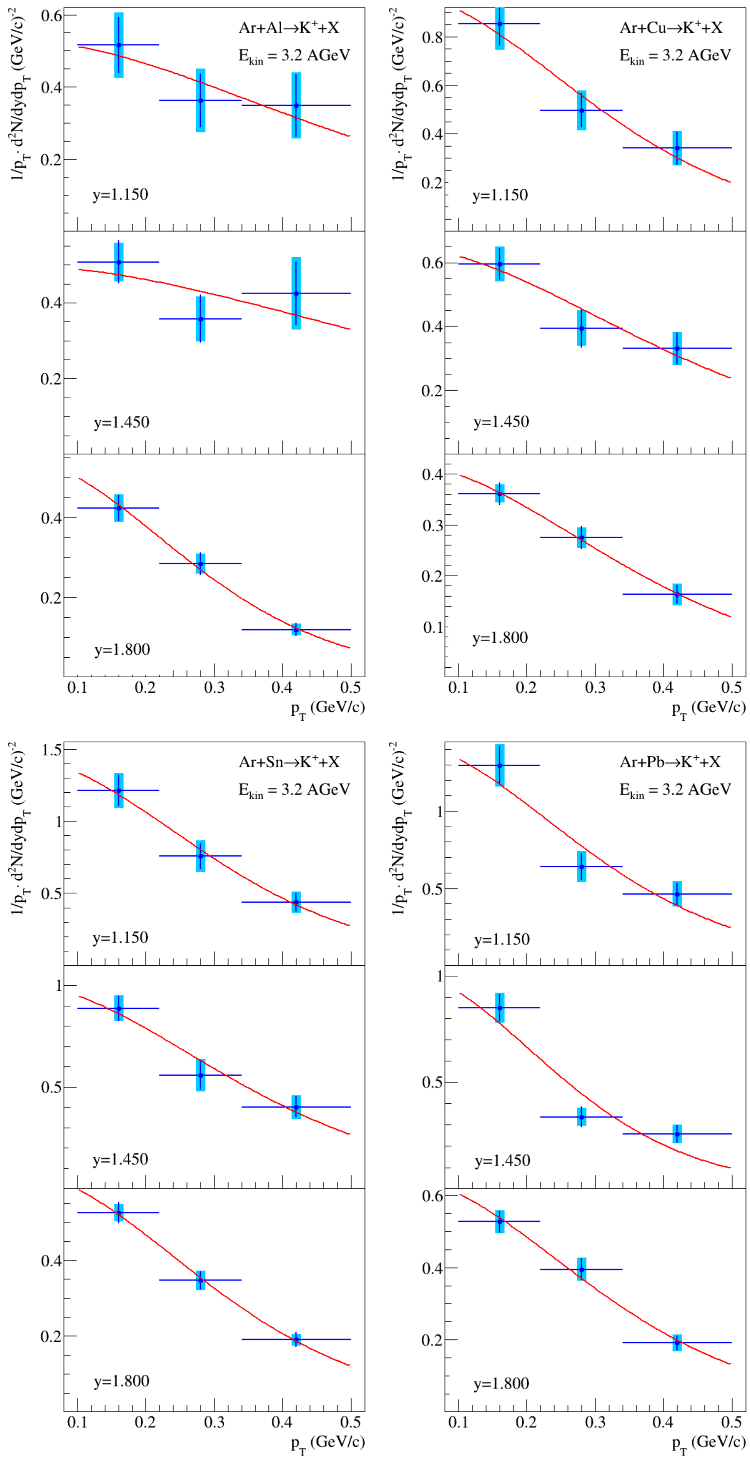

Figure 12: Invariant transverse momentum spectra (p_T) of K^+ mesons produced in Ar+Al, Cu, Sn, Pb interactions at the argon beam energy of 3.2 AGeV. The results are given for three bins of K^+ meson rapidity. The error bars represent the statistical errors, the boxes show the systematic errors. The lines represent the results of the parameterization described in the text.

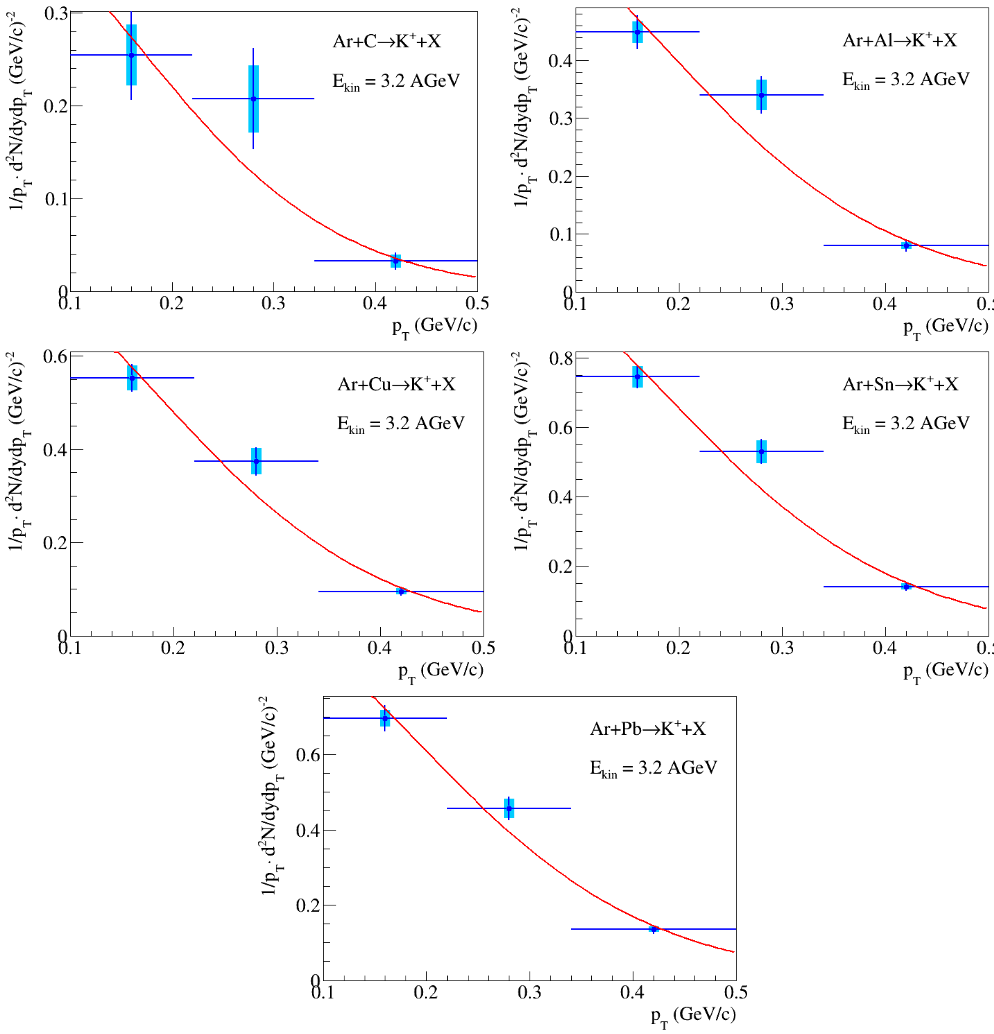

Figure 13: Invariant transverse momentum spectra (p_T) of K^+ mesons produced in Ar+C, Al, Cu, Sn, Pb interactions at the argon beam energy of 3.2 AGeV. The results are given for the measured K^+ meson rapidity range. The error bars represent the statistical errors, the boxes show the systematic errors. The lines represent the results of the parameterization described in the text.

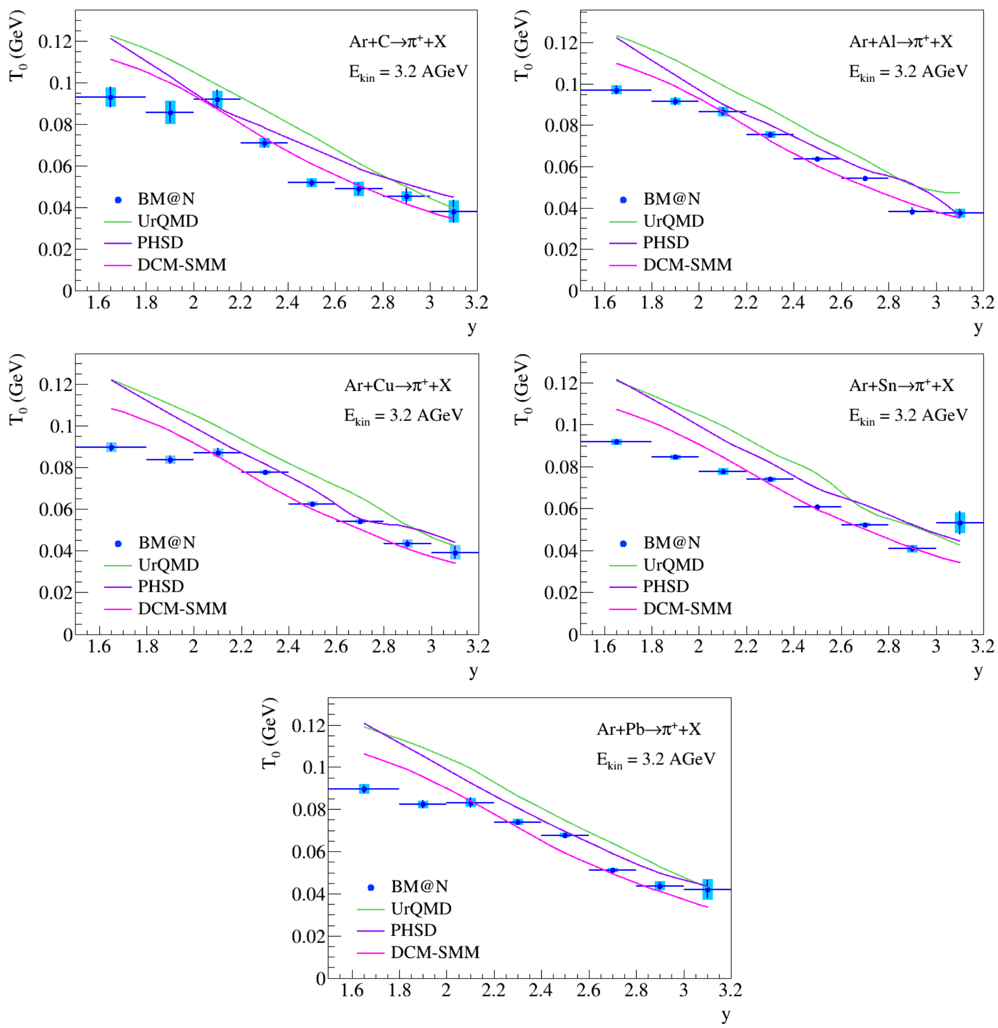

Figure 14: Rapidity y dependence of the inverse slope T_0 extracted from the fits of the π^+ p_T spectra in Ar+C, Al, Cu, Sn, Pb interactions. The error bars represent the statistical errors, the boxes show the systematic errors. The predictions of the DCM-SMM, UrQMD and PHSD models are shown as rose, green and magenta lines.

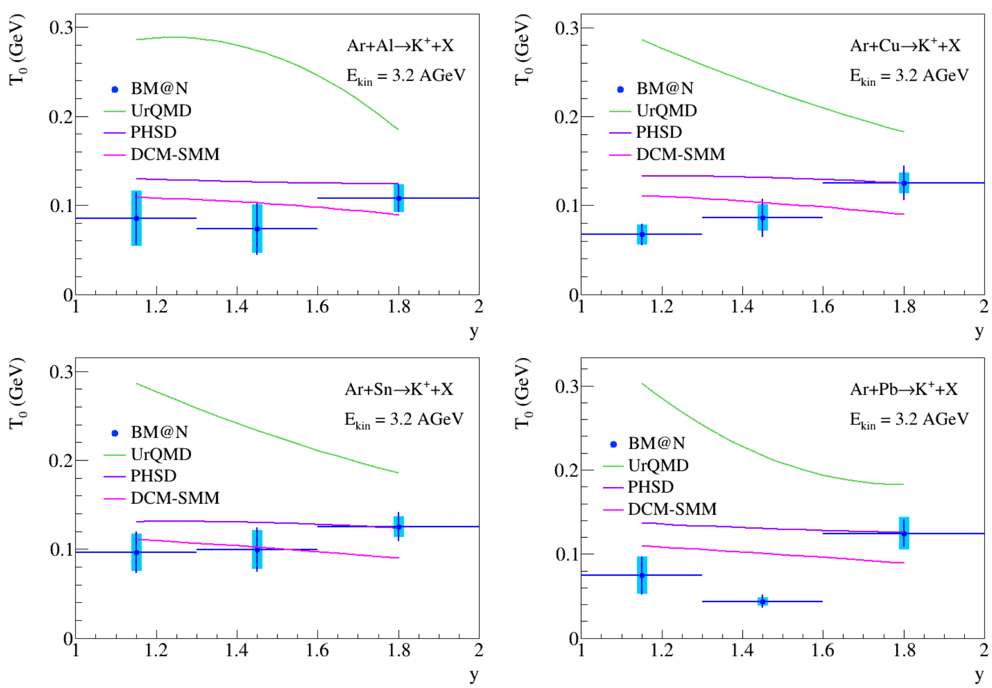

Figure 15: Rapidity y dependence of the inverse slope T_0 extracted from the fits of the K^+ p_T spectra in Ar+Al, Cu, Sn, Pb interactions. The error bars represent the statistical errors, the boxes show the systematic errors. The predictions of the DCM-SMM, UrQMD and PHSD models are shown as rose, green and magenta lines.

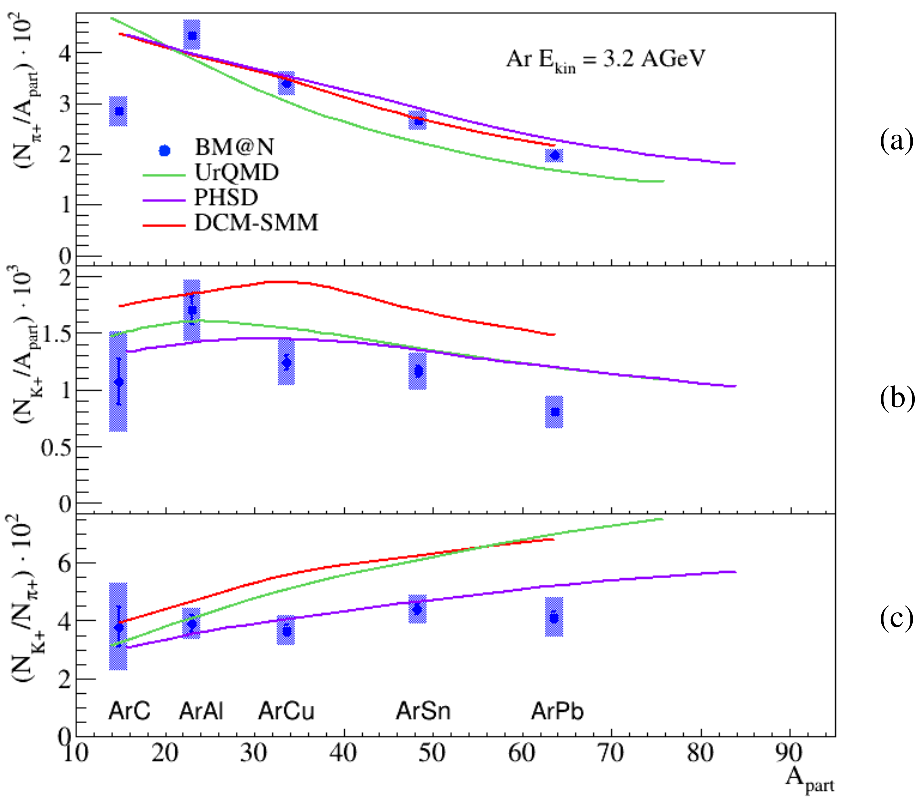

Figure 16: Ratios of the π^+ (a) and K^+ (b) multiplicities to the number of nucleons-participants and ratios of the K^+ to π^+ multiplicities (c) in the measured kinematical range in Ar+C, Al, Cu, Sn, Pb interactions. The error bars represent the statistical errors, the blue boxes show the systematic errors. The BM@N results are compared with predictions of the DCM-QGSM, UrQMD and PHSD models for argon-nucleus interactions shown as red, green and magenta lines.

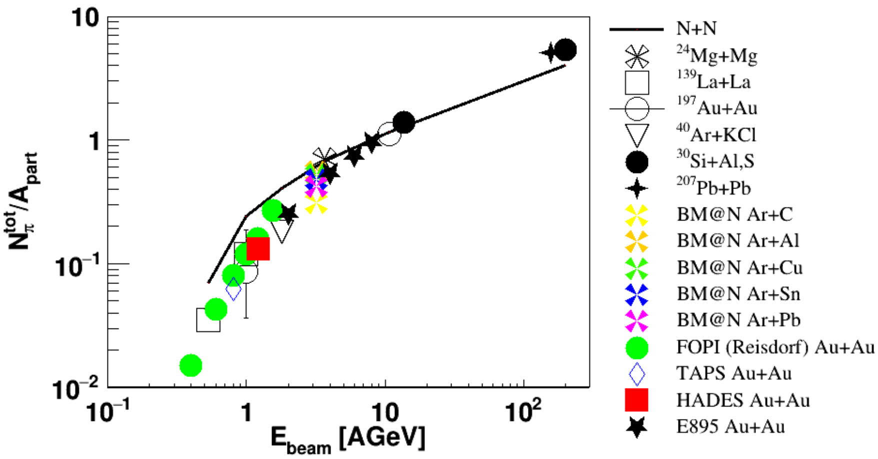

Figure 17: Pion multiplicity N_π^{tot} per the mean number of nucleons-participants $A_{\rm part}$ shown as a function of the beam kinetic energy $E_{\rm beam}$. The BM@N results are compared with the world measurements (references in the text).

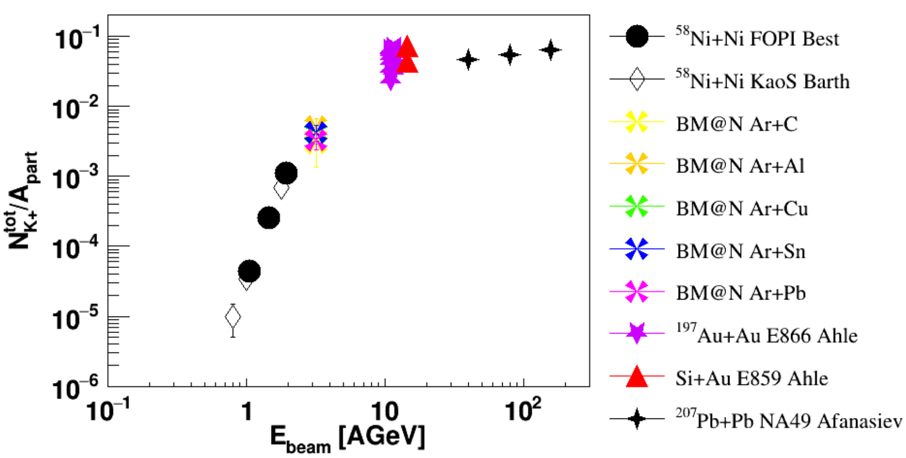

Figure 18: K^+ multiplicity per the mean number of nucleons-participants $A_{\rm part}$ shown as a function of the beam kinetic energy $E_{\rm beam}$. The BM@N results are compared with the world measurements (references in the text).